Parallel-tempering Monte Carlo simulations of the finite temperature behavior of $(H_2O)_6^-$

F. Wang[a)] and K. D. Jordan
Department of Chemistry and Center for Molecular and Materials Simulations, University of Pittsburgh, Pittsburgh, Pennsylvania 15260

The parallel-tempering Monte Carlo method is used in combination with a Drude model to characterize the $(H_2O)_6^-$ cluster over the 50–190 K temperature range. Chainlike structures are found to account for about 50% of the population at 190 K, whereas they are unimportant at the temperatures below about 130 K. At the lowest temperature considered, prismlike structures are dominant. Two new low-energy forms of $(H_2O)_6^-$ are identified. © *2003 American Institute of Physics.* [DOI: 10.1063/1.1624597]

I. INTRODUCTION

Electrons in bulk water are of fundamental importance in radiation chemistry, electrochemistry, and biochemistry.[1–5] The hydrated electron has been known since the early 1960s.[6] Anionic water clusters were first observed mass spectroscopically by Haberland and co-workers in 1984.[7] The $(H_2O)_n^-$ mass spectrum is dominated by peaks at n = 2, 6, 7, and $\geqslant 11$.[7–9] The origin of this intensity pattern is still under debate. Recent advances in vibrational predissociation spectroscopy using Ar solvation techniques have allowed the vibrational spectra of the $n = 5 - 9$ anionic water clusters to be determined in the OH stretch region.[10,11] The vibrational spectra of the $(H_2O)_n^-$ clusters in this size range are similar in appearance, suggesting a common structural motif. Ayotte *et al.*[11] have proposed that chainlike structures are responsible for the observed spectra, but alternative structures have been proposed.[12–14]

Although water clusters do not have low-lying unfilled valence orbitals, an excess electron can bind when the water monomers are arranged so that a sufficiently attractive electrostatic potential results. In those cases that the monomer dipoles are arranged so that the net dipole is in excess of about 2.5 D, an excess electron can bind to give a so-called dipole-bound anion.[15–20] It was long believed that theoretical methods allowing for the electrostatic interactions, and, perhaps also, polarization of the water molecules by the excess electron, were adequate for describing $(H_2O)_n^-$ species.[16,17,21–25] This led researchers to believe that the Hartree–Fock method should provide a good description of the wave functions and of the electron binding energies of these species. This expectation has also served as the basis of several one-electron model approaches that have been developed for describing an excess electron interacting with water.[21,22,24–26] These model potentials have been used in Monte Carlo and molecular dynamics simulations (MD) of excess electrons interacting with bulk water, water films, and water clusters.[27–32]

Over the past few years it has been realized that dispersion interactions between an excess electron and the polar molecules in a cluster play a major role in the electron binding.[33–40] Such interactions are obviously absent in the Hartree–Fock method and in traditional one-electron models. Indeed, it has been found that, within an *ab initio* framework, coupled-cluster CCSD(T) (Ref. 41) or CCSDT calculations using large, flexible basis sets are required to adequately describe the effects of dispersion in these systems.[33–39] *Ab initio* calculations at this level are computationally prohibitive for water clusters containing more than six molecules. As a result, Monte Carlo or MD simulations on $(H_2O)_n^-$ clusters based on accurate *ab initio* energetics (and also forces, in the case of MD simulations) are out of the question.

Recently, we introduced a new one-electron model for describing an excess electron interacting with polar molecules.[20,42,43] This model, which employs quantum Drude oscillators to describe dispersion interactions, gives electron binding energies comparable to those from *ab initio* CCSD(T) calculations, while requiring orders of magnitude less CPU time. In the present work, the Drude model is used to carry out parallel-tempering Monte Carlo simulations[44] on $(H_2O)_6^-$. Several modifications to the original Drude model for $(H_2O)_n^-$ clusters which lead to a significant speedup of the calculations are described.

II. DRUDE MODEL

A. Drude model for electron–molecule interactions

The Drude model was originally introduced to describe the dispersion interactions between atoms or molecules.[45] In this model, two charges, $+q$, and $-q$, coupled harmonically through a force constant k, are placed on each atom or molecule. q and k are generally chosen so that q^2/k, the polarizability (α) of the Drude oscillator, corresponds to the experimental polarizability of the atom or molecule of interest. In a quantum mechanical treatment, a London-type expression is obtained for the dispersion interaction between the oscillators.

In extending this approach to electron–polar molecule

[a)]Present address: Department of Chemistry, University of Utah, Salt Lake City, Utah 84112.

interactions, we introduced a coupling term of the form

$$V^{eD} = \frac{q\mathbf{r}\cdot\mathbf{R}}{r^3} f(r) \qquad (1)$$

between the excess electron and a Drude oscillator.[42,43] Here $\mathbf{R}$ is the vector giving the position of the $+q$ charge of the Drude oscillator relative to the $-q$ charge, which is held fixed, $\mathbf{r}$ is the position vector of the electron relative to the center of the Drude oscillator, and $f(r)$ is a damping function, chosen to be $[1-\exp(-br^2)]$, and used to cut off the unphysical short-range interactions.[46] [Atomic units are employed in Eq. (1) and in subsequent equations.] V^{eD} was combined with a model Hamiltonian, H^{el}, allowing for the interaction of the excess electron with a point-charge representation of the permanent charge distribution of the polar molecules and using pseudopotentials to represent the short-range repulsive interactions between the excess electron and the electron distributions of the monomers. The full system was described by the Hamiltonian

$$H = H^{\text{el}} + H^{\text{osc}} + V^{eD} + V^{DD}, \qquad (2)$$

where H^{osc}, V^{eD}, and V^{DD} were summed over all the Drude oscillators in the system, and V^{DD} allowed for interactions between the Drude oscillators.

In solving the resulting one-electron Schrödinger equation, a product basis of the form $|\phi_i(\mathbf{r})\chi_j^{(1)}(\mathbf{R}_1) \times \chi_k^{(2)}(\mathbf{R}_2)\cdots\rangle$, where ϕ_i is a Gaussian-type electron orbital and $\chi_j^{(m)}(\mathbf{R}_m)$ is the jth eigenfunction associated with the mth Drude oscillator, was used. Details on the oscillator and electron basis sets are given below. The electron binding energy was obtained by use of a configuration interaction singles-plus-doubles (CISD) calculation, where the double excitations allowed for simultaneous excitations of the excess electron and one of the oscillators.

B. Drude model for water

In applying the Drude model to water, the polarizable Dang–Chang (DC) water model,[47] which has been found to provide a good description of neutral water clusters,[47–49] was employed to represent water–water interactions.[20,43] The DC model employs a positive charge (0.519) on each H atom and a negative charge (-1.038) on the rotational axis, but displaced off the O atom toward the H atoms by 0.215 Å. The DC model also associates a Lennard-Jones site with the O atom of each monomer and an isotropic polarizable site at the same location as the negative charge. The DC model gives a binding energy of -4.69 kcal/mol,[47] somewhat smaller than the current best estimates of -4.8 to -5.1 kcal/mol, of the binding energy of the water dimer.[50–54]

In our modification of the DC model for treating excess electron–water interactions, the polarizable site was replaced with a Drude oscillator with the same polarizability. The polarization and dispersion interactions between the excess electron and the oscillators were treated quantum mechanically. Intermolecular induction between the water molecules was also treated quantum mechanically and incorporated by iteratively updating the ground state wave function of the

Drude oscillators (as described by $H^{\text{osc}} + V^{DD}$) until convergence was reached. This procedure gave net (permanent plus induced) dipoles on each water molecule in the cluster nearly identical to those calculated by solving the classical polarization problem for the original DC model.

The electronic Hamiltonian including the contributions from the induced dipoles has the form

$$H^{\text{el}}_{\text{cm}} = -\frac{1}{2}\nabla^2 - \sum_j \frac{Q_j}{r_j} + V^{\text{rep}} + \sum_i \langle 0_i|V^{eD}|0_i\rangle, \qquad (3)$$

where the first sum is over the charge sites of the monomers and the second, which describes the coupling of the excess electron to the induced dipoles, is over the Drude oscillators. The subscript "cm" refers to the choice of atomic charges used in the model. $H^{\text{el}}_{\text{cm}}$ was combined with V^{eD} to give the Drude model for the excess electron. Even though the final Drude model for water employed the DC charges, for the purpose of comparing with *ab initio* Koopmans' theorem (KT) (Ref. 55) calculations and for determining the repulsive potential, it was also useful to consider a model employing charges derived from Hartree–Fock calculations on the water monomer. V^{rep} was derived following the procedure of Schnitker and Rossky.[22] With this choice of V^{rep}, the excess electron is too weakly bound. To remedy this, the repulsive core was scaled so that for the water dimer the electron binding energy obtained from Eq. (3) with the Hartree–Fock charge model reproduces the *ab initio* KT result.

C. Modified Drude model for water

With the original Drude model for electron–water systems, the most CPU-demanding step is the formation of the CISD matrix and the determination of its lowest eigenvalue. The size of the CISD matrix is of the order $N_{\text{osc}}\cdot n_o\cdot n_e$, where N_{osc} is the number of oscillators, n_o is the number of basis functions associated with each oscillator, and n_e is the number of electronic basis functions. Our earlier work employed ten harmonic oscillator basis functions of the form $x^i y^j z^k e^{-\beta(x^2+y^2+z^2)}$, where $0 \le i+j+k \le 2$, for each Drude oscillator. Since the electron is weakly bound in a spatially extended orbital, a flexible electronic basis set is required. Based on the strategy for choosing the electronic basis set used in our earlier study of $(H_2O)_2^-$, $(H_2O)_3^-$, and $(H_2O)_4^-$, it is anticipated that 80–90 Gaussian basis functions would be required to treat the binding of an excess electron to a cluster the size of $(H_2O)_6$. With these basis sets, the dimension of the CI matrix for $(H_2O)_6^-$ is on the order of 5000. Monte Carlo simulations requiring construction of a matrix of this size and extraction of its lowest eigenvalue at each step would be computationally prohibitive, particularly if the simulations were to be run long enough to ensure convergence.

Significant reduction in CPU time would result were it possible to employ only four, i.e., s, p_x, p_y, p_z-like basis functions per oscillator. However, test calculations reveal that large errors result in the calculated dispersion energies when this smaller basis set is used for the oscillators. This is on account of the dual role of the oscillators in describing intramolecular induction and electron–molecule dispersion.

J. Chem. Phys., Vol. 119, No. 22, 8 December 2003

Finite temperature behavior of $(H_2O)_6^-$ 11647

In essence, the induction interactions cause a mixing between the s and p oscillator functions, which, in turn, makes excitations into d-like oscillator functions important for describing electron–water dispersion interactions. This analysis suggests that the errors due to the use of the four-function oscillator basis set would be significantly reduced were the intramolecular induction described classically and the quantum Drude oscillators used to describe the electron–oscillator interactions only. In this approach, the electronic Hamiltonian becomes

$$H_{cm}^{el'} = -\tfrac{1}{2}\nabla^2 - \sum_j \frac{Q_j}{r_j} + \sum_i \frac{\mu_i \cdot r_i}{r_i^3} + V^{rep}, \qquad (4)$$

where μ_j is the induced dipole moment on the jth water molecule calculated by solving the classical self-consistent polarization equations, and V^{eD} describes only the polarization and dispersion interactions between the excess electron and the Drude oscillators.

Test calculations on various $(H_2O)_6^-$ isomers reveal that the modified Drude model with the smaller oscillator basis set gives nearly the same electron binding energies as the original approach [Eq. (3)] in which both intramolecular induction and electron–molecule polarization and dispersion were treated quantum mechanically using Drude oscillators and ten basis functions were employed per oscillator. The adoption of the modified Hamiltonian and the smaller four-function oscillator basis set resulted in over an order of magnitude reduction in the CPU time. Further performance improvement resulted from implementing a semidirect CI method to obtain the lowest eigenvalue of the CI matrix. With these changes, the time to form the CISD matrix and to determine its lowest eigenvalue for a cluster of the size $(H_2O)_6^-$ is reduced to about 1 s on a 2 GHz Pentium 4 computer. However, the total CPU time for the calculation, including evaluation of the integrals over the repulsive cores, is about 10 s.

As will be discussed below, a multicenter expansion of Gaussians was used as the basis set for the excess electron. To facilitate integral evaluation, the repulsive core was also represented in terms of Gaussian functions. The CPU timings cited above were obtained using on each water monomer the 59-Gaussian function representation of the repulsive core developed in Ref. 42. With this choice, a large number of three-center integrals involving the repulsive core and the electronic basis functions result, making this the most time consuming part of the calculation after the changes described above have been implemented to speed up the formation of the CI matrix and the determination of the lowest eigenvalue. To address this problem, a new repulsive core with only three s Gaussians on each H atom and no functions on the O atom was developed. The new repulsive core was scaled so that the electron-binding energy for $(H_2O)_2^-$ obtained using Eq. (4) with Hartree–Fock charges reproduced the electron binding energy from the *ab initio* KT-level calculations. For the larger $(H_2O)_n^-$ clusters, the electron binding energies obtained using the new repulsive core are nearly identical to those obtained using the 59-function representation of the repulsive core. All results discussed below were obtained using the new repulsive core. With the modified Drude

model and the simplified repulsive core, the total CPU time for an energy evaluation for $(H_2O)_6^-$ is about 2 s on a 2 GHz Pentium 4 PC.

D. Basis set and parameters

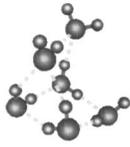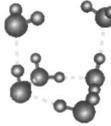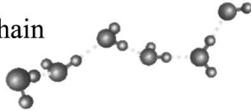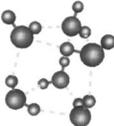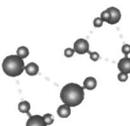In describing the binding of excess electrons to water clusters, large, flexible electronic basis sets must be employed. When using localized basis functions, as in this work, there is the problem of where these functions should be centered. This is particularly problematical for Monte Carlo (or molecular dynamics) simulations exploring a wide range of geometrical configurations. For example, in our $T = 190$ K Monte Carlo simulations of $(H_2O)_6^-$, the dipole moment of the neutral cluster varies from almost zero to about 10 Debye, and, thus, the basis set must be flexible enough to allow for a wide range of spatial distributions of the excess electron. At the same time, the number of basis functions has to be kept as small as possible to minimize computational cost. One approach would be to locate a large set of s and p Gaussian functions on each monomer. Such an approach would be both very demanding computationally and prone to linear dependency. The alternative of putting a large set of Gaussian functions on a single center would require inclusion of very high angular momentum functions to converge the electron binding energy for an arbitrary geometry and thus would also be computationally demanding. A compromise, which works well for many systems, is to combine a large single-center expansion of diffuse s and p functions, perhaps floating, with smaller sets of s and p functions associated with each monomer.

In our initial application of the Drude model to water clusters, the large single-center expansion of s and p functions was augmented with a $2s2p$ set of Gaussian functions on each H atom. In the present study, this $2s2p$ basis set was replaced by a $2s1p$ basis set, reducing the overall CPU time for a Drude model calculation on $(H_2O)_6^-$ by about a factor of 2. The exponents of the two s Gaussian functions, 0.1027, and 0.02526, were taken from our earlier work, as was the exponent of the p function (0.141). In the latter case, the tighter p function was retained. In order to compensate for the small ($\sim 5\%$) decrease in electron binding energies due to the removal of the second p function on each H atom, the repulsive scaling factor and the damping parameter b were adjusted slightly so that the electron binding energies of $(H_2O)_2^-$ calculated using the Drude model, with and without inclusion of dispersion interactions, reproduced the corresponding values obtained with the original Drude model using the larger $2s2p$ basis set on each H atom. (The same large single-center electron basis set was used in both cases.)

For the Monte Carlo simulations described below, the single-center set of diffuse functions was chosen to consist of an even-tempered sequence of five s functions, with exponents ranging from 7.5×10^{-2} to 1.2×10^{-4}, together with an even-tempered sequence of four p functions with exponents ranging from 6.0×10^{-2} to 4.8×10^{-4}, both located at the center of mass of the cluster.

Table I compares the electron binding energies for five isomers of $(H_2O)_6^-$ calculated using the modified Drude

TABLE I. Electron binding energies (in meV) and total energies (in kcal/mol) relative to dbs4dbs2 isomer calculated for selected $(H_2O)_6^-$ isomers.[a,b]

Isomer	Theory	Binding Energy		Relative
		KT	with correlation	Energies
dbs4dbs2	Ab initio	256	465	0.00
	Drude-big	243	483	0.00
	Drude-sm	202	441	0.00
tweezers	Ab initio	312	605	3.52
	Drude-big	272	579	3.73
	Drude-sm	241	558	3.24
chain	Ab initio	230	381	8.83
	Drude-big	205	369	8.95
	Drude-sm	135	299	9.59
dbs3dbs3	Ab initio	185	342	0.43
	Drude-big	186	394	1.96
	Drude-sm	150	363	1.72
se3se3	Ab initio	194	549	10.81
	Drude-big	182	573	9.78
	Drude-sm	184	569	8.90

[a]The *ab initio* electron binding energies are from Ref. 58. The results including electron correlation were obtained at the CCSD(T) level of theory.
[b]Drude model calculations used geometries from Ref. 58 adjusted so that the monomers were restored to the geometries of an isolated, undistorted monomer. The two sets of Drude model results differ in terms of the size and location of the large single-center expansion of diffuse s and p functions. The Drude-big calculations use a large $8s7p$ single-center expansion, the center of which was optimized. The Drude-sm calculations used the smaller $5s4p$ single-center expansion described in the text and located at the center of mass.

model in conjunction with either the $5s4p$ single-center expansion described above or with a larger $8s7p$ single-center expansion, the location of which was variationally optimized. (In both cases, the electronic basis set also included two s functions and one p function on each H-atom as described above.) Excellent agreement is found between the electron binding energies calculated using the Drude model with the $8s7p$ basis set and those obtained from *ab initio* calculations. The Drude model calculations reveal that the dispersion and higher-order contributions to the electron binding energies are exceedingly important, ranging from 164 to 391 meV, depending on the isomer. It is also found that the Drude model employing the smaller single-center expansion, located at the center of mass of the cluster, underestimates the electron binding energies. However, with the exception of the chain isomer, the errors in the electron binding energies due to the restrictions on the electronic basis set are small ($<10\%$). For the chain isomer, the error is 19% (70 meV), reflecting the inadequacy of the relatively small ($5s4p$) single-center basis set, when located so far (≈ 7 Å) from the terminal acceptor water monomer. None-

theless, the smaller $5s4p$ single-center expansion should suffice for the purpose of the Monte Carlo simulations, which are intended to provide semiquantitative information on the relative populations of different isomers as a function of temperature.

From Table I it is also seen that overall the Drude model does a fairly good job at reproducing the relative energies of the different isomers of the anionic isomer as obtained from the CCSD(T) calculations. However, the Drude model predicts the dbs3dbs3 isomer to be 2.0 kcal/mol less stable than dbs4dbs2 isomer in contrast to the 0.4 kcal/mol energy difference from the *ab initio* CCSD(T) calculations. Similarly, the Drude model predicts the se3se3 isomer to be about 1.0 kcal/mol more stable than do the CCSD(T) calculations, which is not of major concern since this is a relatively unstable isomer. These discrepancies arise from the inadequacies of the underlying DC water molecule for describing the neutral clusters in these geometrical arrangements rather than from an inadequacy of the Drude model for describing the interaction of the excess electron with the water cluster.

III. PARALLEL-TEMPERING SIMULATIONS

The Monte Carlo simulations were carried out using the parallel-tempering algorithm[44] to avoid quasiergodic behavior caused by large energy barriers. With this algorithm, simulations for a series of replicas (each at a different temperature) are carried out in parallel, with most attempted moves being confined to individual replicas and carried out using the Metropolis algorithm. The remaining attempted moves involve exchanges of configurations from replicas at adjacent temperatures. The acceptance criterion used for these moves assures that detailed balance is obeyed.[44]

The parallel-tempering simulations of $(H_2O)_6$ and $(H_2O)_6^-$ were initially carried out at eight temperatures between 50–190 K, chosen in a geometric ratio.[56] The highest temperature was chosen so that potential energy barriers are readily overcome. These initial simulations revealed that for the anion the populations are very different at the two highest temperatures, 157 and 190 K. As a result, an additional replica with a temperature of 170 K was added. All simulations described below were carried out using this set of nine replicas. Exchanges between adjacent replicas were attempted every 60 trial moves, and acceptance ratios of 30%–50% were achieved for exchanges of configurations.

The water monomers were kept rigid at the DC geometry. Each individual Metropolis trial move involved either a translation or a rotation of one or more water molecules. Both the number of water monomers and the specific water monomers in the moving unit were chosen at random. The maximum translational and rotational steps were chosen so that an acceptance ratio around 0.5 for the Metropolis algorithm was achieved. The simulations were done in blocks of 500 000 steps. After each simulation block, the saved configurations were scanned for evaporative events. The only evaporative event detected, was that for the $T = 190$ K replica in the simulation on the neutral cluster. In that case, the block of 500 000 configurations experiencing the evaporative event was excluded from the averaging, and the simulation was restarted using a different random number sequence.

In simulating the anionic water clusters, there is the possibility of sampling configurations for which the "anion" lies energetically above the neutral cluster (at the same geometry). Such configurations would be subject to electron autoionization, giving the neutral cluster plus a free electron. In our simulations the electron cannot escape to an infinite distance from the cluster due to the constraints of the basis set. This, of course, could make recapture processes more prevalent than in the experiments.

The initial geometries for the simulations were chosen at random. The simulations were pre-equilibrated for 1 500 000 steps, after which the average potential energy and heat capacity at each temperature were no longer rapidly changing. The production runs were carried out for 1 000 000 steps at each temperature, with configurations being saved for subsequent analysis every 500 steps.

In the simulations of the anion, the electron binding energy was recalculated only if change of the dipole moment of the associated neutral cluster for an individual move or for a sequence of consecutive moves exceeded 2% in magnitude.

For dipole moment changes smaller than this, the total energy of the anionic cluster was estimated by adding to the energy of the neutral cluster at the present geometry the electron binding energy from the previous step. (In the event that the step in question involved an exchange move, then the electron binding energy used was that for the previous configuration from the replica with which the exchange was made.) This strategy was motivated by the observation, that, in general, for moves for which the dipole moment is not appreciably altered, the changes in the total energy tend to be dominated by the energy changes associated with the neutral cluster. In order to deal with the possibility that two completely different structures with similar dipole moments are connected by a sequence of intermediate configurations with similar dipole moments, the electron binding energies were always recalculated after ten consecutive trial moves even if the dipole moment did not change by more than 2%. This strategy led to a factor of 2 savings in CPU time for the high-temperature simulations and a factor of 5 savings for the low-temperature simulations of the anionic clusters. This was taken into account in distributing the various replicas over CPUs so as to minimize idle cycles. For the saved geometries, the electron binding energies were recalculated and compared with those estimated using the procedure described above. These calculations show that the errors in the electron binding energies and in total energies due to reuse of the electron binding energies from previous steps never exceeded 5% and 2%, respectively.

IV. RESULTS AND DISCUSSION

Of particular interest are the populations of various forms of $(H_2O)_6$ and $(H_2O)_6^-$ as a function of temperature. We first attempted to characterize the populations by determining the inherent structures,[57] obtained by optimizing the sampled configurations to the "closest" local minima. This was accomplished by means of line searches in conjugate directions. However, this approach was found to undercount the chainlike structures for the anionic clusters since most such structures collapsed to nonchain structures during the minimization procedure. To address this problem, we used instead an order parameter based on a linear combination of the three principle moments of inertia to aid in distinguishing structures. The moment of inertia tensor was calculated using as coordinates the centers of mass of monomers. The origin was taken to be the center of the mass of the entire cluster, and the principle axes were chosen so that the off-diagonal elements of the inertia tensor were zero. The quantity $J_z = \sqrt{\frac{1}{2}(A+B-C)}$, where A, B, and C are the three principal moments as usually defined ($A \geqslant B \geqslant C$), was calculated. The motivation for this combination was that J_z can readily distinguish prism and cage structures and also separates the chain from nonchain structures. In calculating the J_z values, the total mass of the water cluster was taken to be one, and the coordinates were in atomic units. Histograms giving the populations as a function of J_z are plotted and analyzed.

Table II reports ranges of J_z values for several isomers for $(H_2O)_6$ and $(H_2O)_6^-$ that acquire significant population

TABLE II. J_z values for selected isomers of $(H_2O)_6^-$.

Isomer[a]	J_z values
prism[b]	$6.0 \leq J_z \leq 7.5$
cage	$7.5 \leq J_z \leq 8.5$
open-book	$8.5 \leq J_z \leq 11.5$
cage+tail	$9.5 \leq J_z \leq 11.5$
ring	$9.0 \leq J_z \leq 10.0$
ring plus tail(s)	$11.0 \leq J_z \leq 16.0$
chain	$J_z \geq 16$

[a]The various structures are defined in Fig. 1.
[b]dbs4dbs2 and dbs4′dbs2 also have J_z values in this range.

in one or more replicas. Selected configurations from the $T = 157$ and 190 K replicas from the parallel-tempering simulations on the anion are depicted in Fig. 1, which also reports the dipole moments, J_z values, and energies. The various clusters shown in the figure are classified as "cage," "prism," "open-book," "cage+tail," "ring+tail," "fused-ring+tail," "chain," "dbs4dbs2," and "dbs4′dbs2." The dbs4dbs2 and dbs4′dbs2 nomenclature, adopted from Ref. 58, implies that these anions are dipole-bound and that the clusters can be viewed as being comprised of a cyclic tetramer, bridged by a water dimer. It should be noted that the structures shown in Fig. 1 have not been optimized to their local minima and that the most stable cage, prism, and open-book structures have different arrangements of the H-bonds in the anionic than in the neutral clusters.

Figure 2(a) reports for the neutral cluster the J_z histograms for a subset of the nine replicas. The areas under the curves were integrated with respect to J_z and the resulting cumulative populations are plotted in Fig. 2(b). In the lowest temperature ($T = 50.0$ and 60.5 K) replicas, most of the population is associated with pronounced peaks near $J_z = 6.5$ and 8.25 which corresponding to prismlike and cagelike structures, respectively, with the latter being more prevalent. At somewhat higher temperatures, a small population of prismlike structures with one broken H-bond and $J_z \sim 7.0$ builds up. As the temperature is further increased, the population shifts mainly to open-book and ring structures ($J_z = 9-11$). These results are consistent with previous Monte Carlo simulations of $(H_2O)_6$.[48] Chainlike structures are not detected for the neutral cluster at temperatures as high as 190 K.

Figure 3(a) reports the J_z histograms for a subset of the nine replicas from the parallel tempering simulations on $(H_2O)_6^-$. The cumulative populations are shown in Fig. 3(b). The J_z distributions for the anion are significantly different from those of the neutral cluster, consistent with the large influence of the excess electron on the morphology of the clusters. At the lowest temperature (50 K) considered, most ($\sim 95\%$) of the population is associated with structures with J_z values close to 6.5, with nearly all of the remaining population being associated with a small peak centered near $J_z = 8.2$. Due to different isomers possessing similar J_z values, it has proven to be necessary to graphically examine the
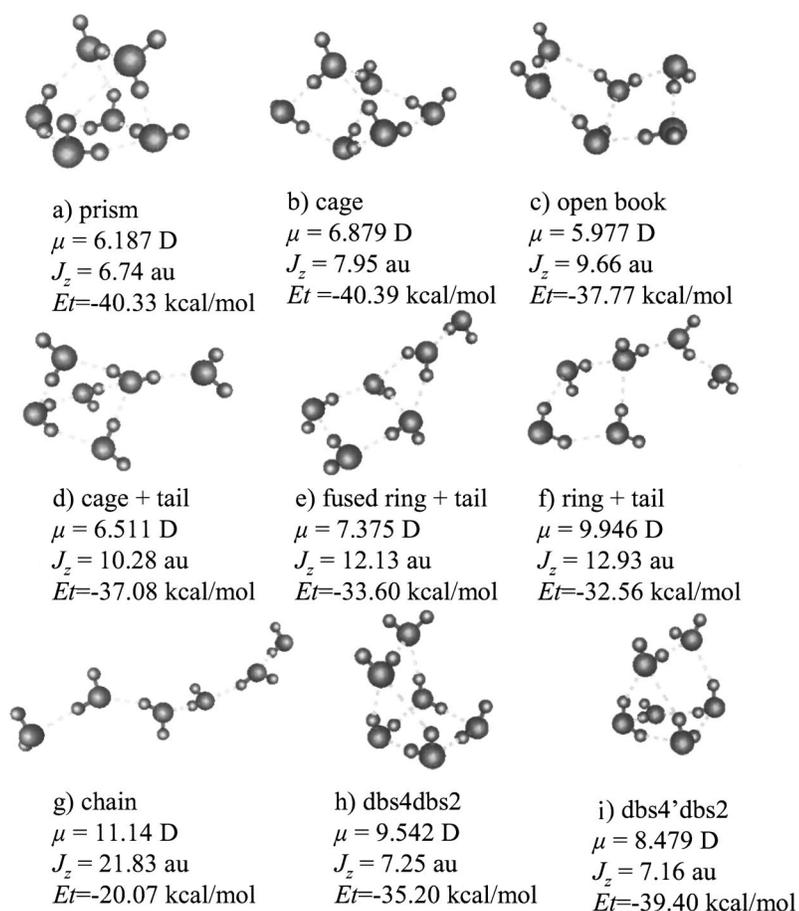

a) prism
$\mu = 6.187$ D
$J_z = 6.74$ au
$Et = -40.33$ kcal/mol

b) cage
$\mu = 6.879$ D
$J_z = 7.95$ au
$Et = -40.39$ kcal/mol

c) open book
$\mu = 5.977$ D
$J_z = 9.66$ au
$Et = -37.77$ kcal/mol

d) cage + tail
$\mu = 6.511$ D
$J_z = 10.28$ au
$Et = -37.08$ kcal/mol

e) fused ring + tail
$\mu = 7.375$ D
$J_z = 12.13$ au
$Et = -33.60$ kcal/mol

f) ring + tail
$\mu = 9.946$ D
$J_z = 12.93$ au
$Et = -32.56$ kcal/mol

g) chain
$\mu = 11.14$ D
$J_z = 21.83$ au
$Et = -20.07$ kcal/mol

h) dbs4dbs2
$\mu = 9.542$ D
$J_z = 7.25$ au
$Et = -35.20$ kcal/mol

i) dbs4'dbs2
$\mu = 8.479$ D
$J_z = 7.16$ au
$Et = -39.40$ kcal/mol

FIG. 1. Representative configurations of $(H_2O)_6^-$ sampled in the 157 and 190 K replicas. Note that these configurations have not been quenched to local potential energy minima.

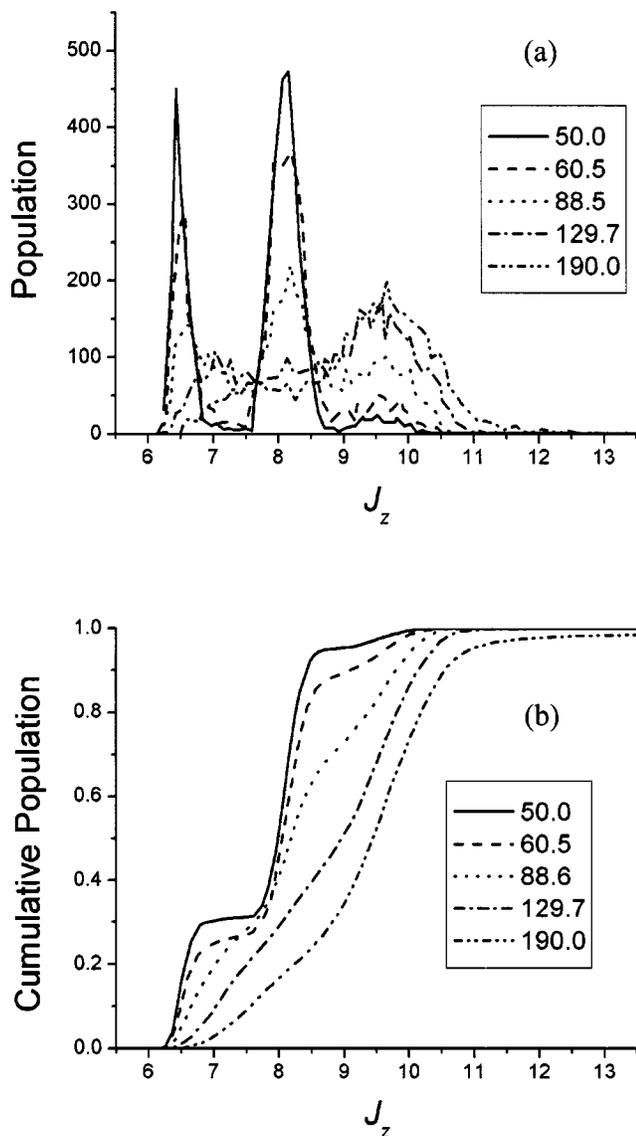FIG. 2. (a) Distribution of $(H_2O)_6$ configurations as a function of J_z. (b) Integration of (a) normalized to 1.0.

FIG. 3. (a) Distribution of $(H_2O)_6^-$ configurations as a function of J_z. (b) Integration of (a) normalized to 1.0.

configurations saved at each temperature in order to establish definitively which isomers are contributing to the various peaks. On this basis, it was determined that the peak near $J_z = 6.5$ is almost entirely due to prismlike structures and that near $J_z = 8.2$ to cagelike structures. As the temperature is increased above 50 K, the prism and cage isomers fall off in importance, and a peak grows in around $J_z = 7$, which corresponds to structures derived from the prism by breaking one or two H-bonds. Inspection of the configurations sampled at $T = 157$, 170, and 190 K reveals that open-book [Fig. 1(c)], cage-plus-tail [Fig. 1(d)], ring-plus-tail [Figs. 1(e), 1(f)], and chainlike structures [Fig. 1(g)] are abundant. At $T = 157$ K the chainlike structures account for only about 5% of the structures, while at $T = 190$ K they account for about 50% of the observed configurations. Due to the limitations of the electronic basis set used for the simulations, the stability of the chainlike isomer at its optimized geometry is underestimated by 0.64 kcal/mol. Thus it is expected that chainlike structures would be somewhat more important at lower tem-
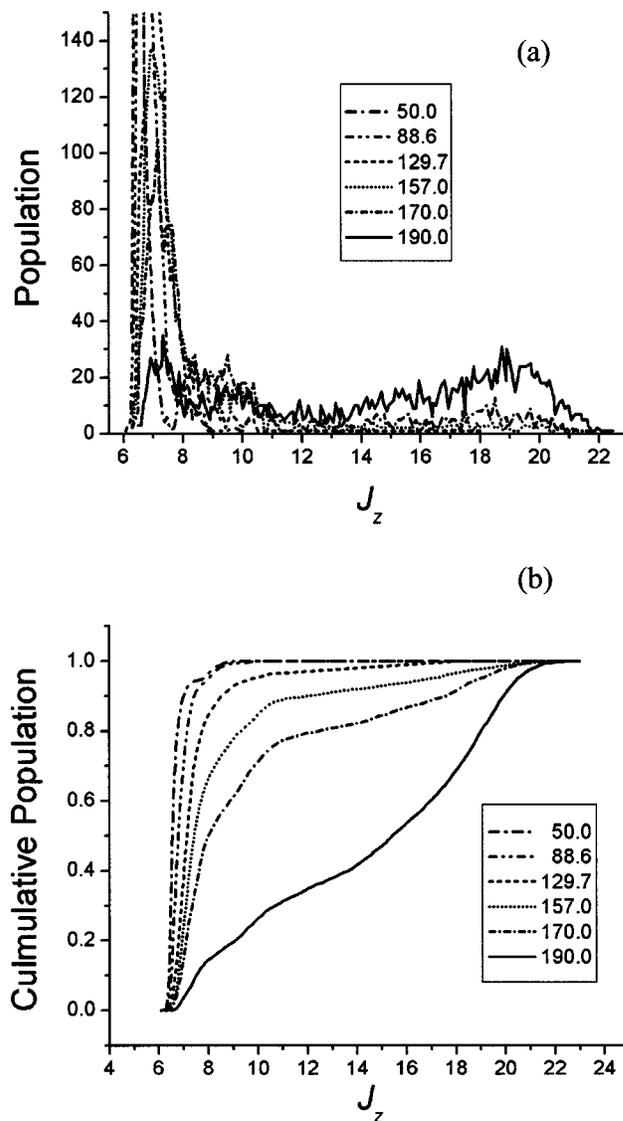
peratures were a more flexible basis set adopted.

These results show that for $(H_2O)_6^-$ there is an evolution from "compact" structures to more "open" structures with increasing temperature. The evolution corresponds to the breaking of hydrogen bonds, with the maximum number (9) of hydrogen bonds being for the prismlike structures that dominate at $T \approx 50$ K, and the smallest number (5) being for the chainlike structures that dominate at high temperatures. (However, as will be seen below, the dbs4dbs2 and dbs4'dbs2 species with eight H-bonds are slightly more stable than the prism isomer.)

Both the tweezers structure[13,59] and the dbs4'dbs2 structure[14] depicted in Figs. 1 and 4 have been proposed for the dominant species observed experimentally. A common feature of these two structures is the presence of a four-membered-ring [with a H-bonding arrangement similar to that of the most stable form of $(H_2O)_4$] at the "bottom" of the cluster and two water molecules on the "top" of the cluster. In the tweezers structure, the two "on-top" mol-

a) prism
$\mu = 6.887$ D
$J_z = 6.31$ au
$Et = -44.27$ kcal/mol

b) cage
$\mu = 7.303$ D
$J_z = 7.82$ au
$Et = -44.38$ kcal/mol

c) dbs4dbs2
$\mu = 9.526$ D
$J_z = 6.70$ au
$Et = -44.52$ kcal/mol

d) dbs4′dbs2
$\mu = 9.611$ D
$J_z = 6.72$ au
$Et = -44.72$ kcal/mol
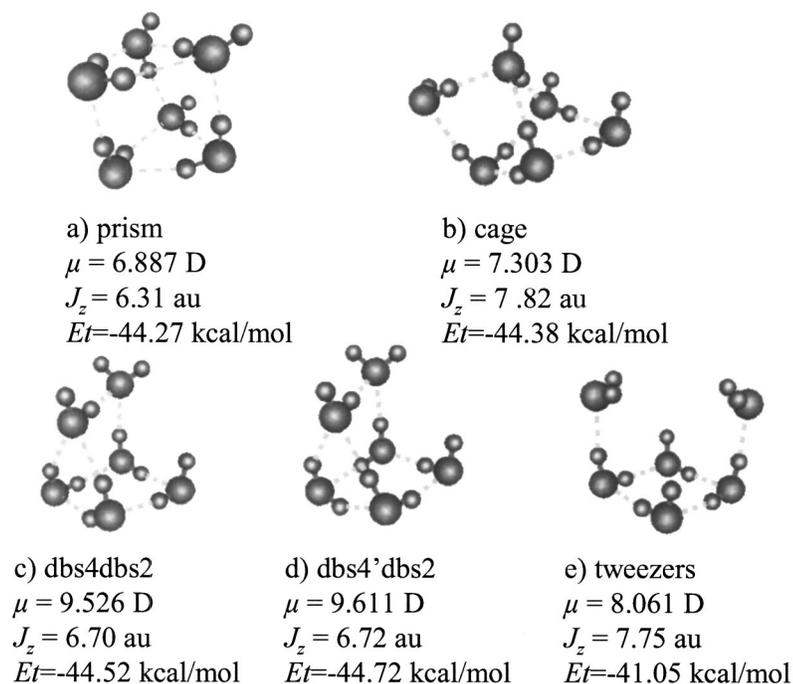
e) tweezers
$\mu = 8.061$ D
$J_z = 7.75$ au
$Et = -41.05$ kcal/mol

FIG. 4. Selected local potential energy minima of $(H_2O)_6^-$ as described by the Drude model. The geometries were optimized using the smaller basis set for the excess electron, followed by single-point calculations of the total energies using the larger basis set.

ecules are not bonded to one another and have their dipoles oriented so that the excess electron can be partially localized between them. In the dbs4′dbs2 structure the two "on-top" monomers are bonded together. The dbs4dbs2 isomer, which is depicted in Fig. 1 and which has been considered by Gutowski, differs from dbs4′dbs2 only in the orientation of the single-donor OH groups of the four-membered ring.

Figure 4 reports the relative energies of the dbs4dbs2, dbs4′dbs2 and tweezers structures as well as of the most stable cage (4b) and prism (4a) structures of $(H_2O)_6^-$ optimized using the Drude model. The most stable isomer of $(H_2O)_6^-$ is predicted to be the dbs4′dbs2 isomer, followed by the dbs4dbs2, cage, prism, and tweezers isomers, lying 0.20, 0.34, 0.45, and 3.67 kcal/mol higher in energy, respectively. The prediction that the global minimum structure is dbs4′dbs2 is in agreement with recent CCSD(T) calculations of Kim et al.[14] The most stable cage and prism structures found in this study have different arrangements of the H-bonds and are more stable than the lowest-energy cage and prism isomers reported by Kim et al.

Visual inspection of the configurations sampled in the parallel-tempering simulations reveals that the dbs4′dbs2, dbs4dbs2, and tweezers species do not acquire sizable population at any of the temperatures considered. At the lowest temperature (50 K) employed in the parallel-tempering simulations, the dbs4dbs2 and dbs4′dbs2, species together account for less than 0.6% of the total population and no tweezers structures are observed over the 50–190 K temperature range. However, the importance of the dbs4dbs2 and dbs4′dbs2 species would increase as the temperature is decreased from 50 K.

V. CONCLUSIONS

Our parallel-tempering Monte Carlo simulations of the $(H_2O)_6^-$ cluster indicate that the chainlike structures, previ-

ously proposed by Ayotte et al. as a being responsible for the observed vibrational spectra of $(H_2O)_6^-$, account for about 50% of the configurations sampled at $T = 190$ K, but drop off rapidly in importance with decreasing temperature, e.g., accounting for only 5% of the population at $T = 157$ K, and having negligible population at temperatures below 130 K. The simulations of the neutral cluster do not reveal any chainlike structures even at temperatures as high as 190 K. The $(H_2O)_6^-$ clusters that were characterized by means of vibrational spectroscopy are believe to have been formed by electron capture by neutral $(H_2O)_6Ar_n$ clusters, which would necessarily have had temperatures well below 50 K. Indeed, many of the observed $(H_2O)_6^-$ clusters had one or more Ar atoms attached. Of course, there is the possibility that cooling of the neutral clusters is so rapid (via collisions and Ar-atom evaporation), that higher-energy structures are frozen in. However, even in that event, it seems unlikely that there would be a significant population of chainlike $(H_2O)_6$ species under experimental conditions. Thus, if the chainlike isomer is responsible for the observed vibrational spectrum of $(H_2O)_6^-$, there remains the puzzle of how it is formed in experiments in which electron attachment occurs to existing water clusters. The present simulations also show that were equilibrium actually achieved for the anionic clusters, then configurations with prismlike structures should dominate at cluster temperatures near 50 K and that the dbs4′dbs2 and dbs4dbs2 structures should dominate at appreciably lower temperatures.

Our Drude model calculations predict the prism [Fig. 4(a)], cage [Fig. 4(b)], dbs4′dbs2 [Fig. 4(d)] and dbs4dbs2 [Fig. 4(c)] isomers of $(H_2O)_2^-$ to be particularly stable. The corresponding calculated vertical electron detachment energies are 368, 426, 619, and 614 meV as compared to the 480 meV experimental value.[10] For the dbs4′dbs2 and dbs4dbs2 species,[14,58] for which the results of high-level ab initio elec-

tronic structure calculations are available, the Drude model calculations (using structures optimized using the Drude model) give VDE's about 35% larger than the high-level *ab initio* values (at *ab initio* optimized geometries). Since, the results reported in Table I show that the Drude model and coupled-cluster-level *ab initio* calculations give similar values for the VDE's providing the same geometries are employed, it appears that geometry differences are primarily responsible for the differences between the VDE's obtained using the Drude model (with geometries optimized with that method) and using *ab initio* calculations (and with *ab initio* optimized geometries). It is not clear whether the Drude-model or the *ab initio* calculations provide more accurate characterization of the geometries of the anions. The main limitation of the *ab initio* calculations, is the use of MP2-optimized structures. Since high-order correlation effects significantly enhance electron binding, we anticipate that they could be important for establishing the geometrical structures as well. On the other hand, the DC model used to describe the water–water interactions in the Drude model calculations may not be adequate for characterizing the geometries of species such as dbs4′dbs2. Given these uncertainties and the sensitivity of the VDE's to the geometries, we conclude that both the low-energy prism and cage forms of $(H_2O)_6^-$ identified in this study have calculated electron binding energies sufficiently close to the 480 meV experimental value, that they could also be viable candidates for the species responsible for the observed vibrational spectrum of $(H_2O)_6^-$. However, the calculated vibrational spectra[60] for these species differ appreciably from the measured spectrum. Additional experimental and theoretical work will be required to establish unambiguously the identity of the isomers responsible for the observed vibrational spectrum of $(H_2O)_6^-$.

ACKNOWLEDGMENTS

[1] R. Laenen, T. Roth, and A. Laubereau, Phys. Rev. Lett. **85**, 50 (2000).
[2] C. Silva, P. K. Walhout, K. Yokoyama, and P. F. Barbara, Phys. Rev. Lett. **80**, 1086 (1998).
[3] D. M. Bartels, A. R. Cook, M. Mudaliar, and C. D. Jonah, J. Phys. Chem. A **104**, 1686 (2000).
[4] R. A. Crowell and D. M. Bartels, J. Phys. Chem. **100**, 17713 (1996).
[5] D. M. Bartels, D. Gosztola, and C. D. Jonah, J. Phys. Chem. A **105**, 8069 (2001).
[6] E. J. Hart and J. W. Boag, J. Am. Chem. Soc. **84**, 4090 (1962).
[7] H. Haberland, H. G. Schindler, and R. Worsnop, Ber. Bunsenges. Phys. Chem. **88**, 271 (1984).
[8] J. Kim, I. Becker, O. Cheshnovsky, and M. A. Johnson, Chem. Phys. Lett. **297**, 90 (1998).
[9] J. V. Coe, G. H. Lee, J. G. Eaton, S. T. Arnold, H. W. Sarkas, K. H. Bowen, C. Ludewigt, H. Haberland, and R. Worsnop, J. Chem. Phys. **92**, 3980 (1990).
[10] P. Ayotte, C. G. Bailey, J. Kim, and M. A. Johnson, J. Chem. Phys. **108**, 444 (1998).
[11] P. Ayotte, G. H. Weddle, C. G. Bailey, M. A. Johnson, F. Vila, and K. D. Jordan, J. Chem. Phys. **110**, 6268 (1999).
[12] K. S. Kim, I. Park, S. Lee, K. Cho, J. Y. Lee, J. Kim, and J. D. Joannopoulos, Phys. Rev. Lett. **76**, 956 (1996).
[13] S. Lee, J. Kim, S. J. Lee, and K. S. Kim, Phys. Rev. Lett. **79**, 2038 (1997).
[14] H. M. Lee, S. Lee, and H. S. Kim, J. Chem. Phys. **119**, 187 (2003); S. B. Suh, H. M. Lee, J. Kim, J. Y. Lee, and K. S. Kim, *ibid.* **113**, 5273 (2000).
[15] W. R. Garrett, Phys. Rev. A **3**, 961 (1971).
[16] K. D. Jordan, Acc. Chem. Res. **12**, 36 (1979).
[17] J. Simons and K. D. Jordan, Chem. Rev. (Washington, D.C.) **87**, 535 (1987).
[18] R. N. Compton and N. I. Hammer, in *Advances in Gas-Phase Ion Chemistry*, edited by N. G. Adams (JAI, Greenwich, 2001), Vol. 4, p. 257.
[19] J. Simons and P. Skurski, in *Theoretical Prospects of Negative Ions*, edited by J. Kalcher (Research Signpost, Trivandrum, 2002), p. 117.
[20] K. D. Jordan and F. Wang, Annu. Rev. Phys. Chem. **54**, 367 (2003).
[21] R. N. Barnett, U. Landman, C. L. Cleveland, and J. Jortner, J. Chem. Phys. **88**, 4421 (1988).
[22] J. Schnitker and P. J. Rossky, J. Chem. Phys. **86**, 3462 (1987).
[23] J. Schnitker and P. J. Rossky, J. Chem. Phys. **86**, 3471 (1987).
[24] A. Staib and D. Borgis, J. Chem. Phys. **103**, 2642 (1995).
[25] A. Wallqvist, D. Thirumalai, and B. J. Berne, J. Chem. Phys. **85**, 1583 (1986).
[26] A. Mosyak, P. Graf, I. Benjamin, and A. Nitzan, J. Phys. Chem. A **101**, 429 (1996).
[27] R. N. Barnett, U. Landman, D. Scharf, and J. Jortner, Acc. Chem. Res. **22**, 350 (1989).
[28] M. Marchi, M. Sprik, and M. L. Klein, J. Chem. Phys. **89**, 4918 (1988).
[29] U. Landman, R. N. Barnett, C. L. Cleveland, J. Luo, D. Scharf, and J. Jortner, in *Few Body Systems and Multiparticle Dynamics*, edited by D. Micha (AIP, New York, 1987), p. 200.
[30] I. Benjamin, D. Evans, and A. Nitzan, J. Chem. Phys. **106**, 6647 (1997).
[31] R. N. Barnett, U. Landman, and A. Nitzan, J. Chem. Phys. **89**, 2242 (1988).
[32] R. N. Barnett, U. Landman, and A. Nitzan, Phys. Rev. Lett. **62**, 106 (1989).
[33] M. Gutowski and P. Skurski, Chem. Phys. Lett. **300**, 331 (1999).
[34] P. Skurski, M. Gutowski, and J. Simons, Int. J. Quantum Chem. **80**, 1024 (2000).
[35] M. Gutowski and P. Skurski, J. Chem. Phys. **107**, 2968 (1997).
[36] K. A. Peterson and M. Gutowski, J. Chem. Phys. **116**, 3297 (2002).
[37] M. Gutowski and P. Skurski, Recent Res. Dev. Phys. Chem. **3**, 245 (1999).
[38] M. Gutowski, K. D. Jordan, and P. Skurski, J. Phys. Chem. A **102**, 2624 (1998).
[39] M. Gutowski, P. Skurski, A. I. Boldyrev, J. Simons, and K. D. Jordan, Phys. Rev. A **54**, 1906 (1996).
[40] M. Sindelka, V. Spirko, and P. Jungwirth, J. Chem. Phys. **117**, 5113 (2002).
[41] J. A. Pople, M. Head-Gordon, and K. Raghavachari, J. Chem. Phys. **87**, 5968 (1987).
[42] F. Wang and K. D. Jordan, J. Chem. Phys. **114**, 10717 (2001).
[43] F. Wang and K. D. Jordan, J. Chem. Phys. **116**, 6973 (2002).
[44] J. P. Neirotti, F. Calvo, D. L. Freeman, and J. D. Doll, J. Chem. Phys. **112**, 10340 (2000).
[45] M. Rigby, E. B. Smith, W. A. Wakeham, and G. C. Maitland, *The Forces Between Molecules* (Clarendon, Oxford, 1986).
[46] This form of the damping function facilitates the evaluation of the integrals over the Gaussian basis functions.
[47] L. X. Dang and T. M. Chang, J. Chem. Phys. **106**, 8149 (1997).
[48] J. M. Pedulla and K. D. Jordan, Chem. Phys. **239**, 593 (1998).
[49] C. J. Burnham and S. S. Xantheas, J. Chem. Phys. **116**, 1479 (2002).
[50] W. Klopper, J. G. C. M. Duijneveldt van de Rijdt, and F. B. van Duijneveldt, Phys. Chem. Chem. Phys. **2**, 2227 (2000).
[51] G. S. Tschumpa, M. L. Leininger, B. C. Hoffman, E. F. Valeev, H. F. Schaefer III, and M. Quack, J. Chem. Phys. **116**, 690 (2002).
[52] N. Goldman, R. S. Fellers, M. G. Brown, L. B. Braly, C. G. Koeshian, C. Leforestier, and R. J. Saykally, J. Chem. Phys. **116**, 10148 (2002).
[53] E. M. Mas and K. Szalewicz, J. Chem. Phys. **104**, 7606 (1996).
[54] S. S. Xantheas, J. Chem. Phys. **104**, 8821 (1996).
[55] T. Koopmans, Physica (Amsterdam) **1**, 104 (1934).
[56] K. Makrodimitris, G. K. Papadopoulos, C. Philippopoulo, and D. N. Theodorou, J. Chem. Phys. **117**, 5876 (2002).
[57] F. H. Stillinger and T. A. Weber, J. Phys. Chem. **87**, 2833 (1983).
[58] M. Gutowski (private communication).
[59] K. S. Kim, S. Lee, J. Kim, and J. Y. Lee, J. Am. Chem. Soc. **119**, 9329 (1997).
[60] F. Wang and K. D. Jordan (unpublished).